




## Modulating the electronic structure and interface contact of $WSe_2/CrSe_2$ van der Waals heterostructures by strain engineering: Insights from first-principles calculations

Fangqi Yu,<sup>1</sup> Weihua Yang,<sup>1</sup> Rao Huang ,<sup>1</sup> Lei Li ,<sup>2</sup> Yang Zhang,<sup>3</sup> and Yuhua Wen ,<sup>1,\*</sup>

<sup>1</sup>Department of Physics, Xiamen University, Xiamen 361005, China

<sup>2</sup>Department of Physics, Inner Mongolia Normal University, Hohhot 010022, China

<sup>3</sup>Department of Applied Physics, Xi'an Jiaotong University, Xi'an 710049, China



(Received 5 October 2023; accepted 21 December 2023; published 10 January 2024)

As a recent member of the two-dimensional (2D) van der Waals (vdW) heterostructures, the  $WSe_2/CrSe_2$  heterostructure has received considerable attention due to its fascinating characteristics compared with the constituent 2D materials. In this paper, we performed first-principles calculations to investigate its structural, electronic, and magnetic properties and explored the effects of interlayer and in-plane strains on these properties. Our results reveal that the antiferromagnetic (AFM) ground state in the  $CrSe_2$  layer of the heterostructure is maintained owing to weak vdW interactions between the  $CrSe_2$  and  $WSe_2$  layers. However, the AFM state can be transformed into the ferromagnetic state at interlayer compressive strain of  $-19\%$  or in-plane tensile strain of  $2.5\%$ . Moreover, the  $WSe_2/CrSe_2$  heterointerface belongs to the metal-semiconductor interface and exhibits  $p$ -type ohmic contact and low contact resistance. The transition from  $p$ -type ohmic contact to  $p$ -type Schottky contact or  $n$ -type Schottky contact can be achieved by interlayer or in-plane strain engineering, which is associated with the strain-induced energy shifts of the valence band maximum and conduction band minimum of  $WSe_2$ . Additionally, the tunneling probability of the heterostructure rises dramatically (up to 100%) with interlayer coupling, which is favorable for carrier transport at the heterointerface. Our findings demonstrate that strain engineering is an effective way of modulating metal-semiconductor interfaces and provide theoretical guidance for designing electronic and magnetic devices based on the  $WSe_2/CrSe_2$  vdW heterostructure as well as broadening its applications in future functional devices.

DOI: [10.1103/PhysRevMaterials.8.014003](https://doi.org/10.1103/PhysRevMaterials.8.014003)

### I. INTRODUCTION

Since graphene was obtained by mechanical exfoliation of graphite [1], ultrathin two-dimensional (2D) nanomaterials have attracted increasing interest from various fields of science and engineering because of their substantial properties and wide application prospects [2–6]. In addition to graphene and its derivatives, transition metal dichalcogenides (TMDs) with the chemical formula  $MX_2$  ( $M = Ti, Zr, Hf, V, Nb, Ta, Cr, Mo, W; X = S, Se, Te$ ), as a family of 2D nanomaterials with favorable electronic properties, have been widely recognized as potential candidates in the fields of field-effect transistors and optoelectronic devices [7–14]. However, no single material can fulfill diverse requirements and be used for multiple purposes. For example, some TMDs exhibit low carrier mobility despite their ideal band gaps, limiting their uses in high-performance electronic and optoelectronic devices [15,16]. Given this, one of the solving strategies for complementing advantages and expanding possibilities is to construct 2D van der Waals (vdW) heterostructures [4,17–19].

Various 2D vdW heterostructures with desired properties have been prepared experimentally [20–25]. Among them, metal-semiconductor vdW heterostructures have been

considered attractive building blocks in 2D electronic and optoelectronic devices [26,27]. As a critical parameter affecting carrier injection in devices, the barrier height at the metal-semiconductor interfaces dominates the carrier injection efficiency and transport performance. However, Fermi-level pinning, lattice strain, and metal-induced gap states at the interfaces can greatly inhibit carrier transport and contact tunability, leading to performance degradation, especially in atomically thin devices [26,28]. Therefore, understanding the metal-semiconductor interface properties and developing interfacial engineering is crucial for the design and realization of metal-semiconductor heterostructures with excellent performance. For this purpose, vertically stacked metal-semiconductor heterostructures based on 2D TMDs are considered one of the candidates. They can form either Schottky or ohmic contacts [29,30]. Furthermore, the interface contact types and associated barriers of these heterostructures can be effectively modulated by strain engineering [31–38]. For example, available experimental studies show that the graphene/ $MoS_2$  heterostructure has ultrahigh strain sensitivity and enables large-scale modulation of the Schottky barrier [32], and the construction of  $MoS_2$  and  $WSe_2$  in field-effect transistors can lower their contact barriers with the source and drain by strain [31,33]. Theoretical calculations also demonstrate that the contact types formed by graphene/ $WSe_2$  and graphene/ $MoS_2$  can be modulated by out-of-plane strain [36]. In-plane strain has also been applied to

\*yhwen@xmu.edu.cn

change the interfacial contact types and tunneling barrier of  $\text{Ti}_3\text{C}_2\text{T}_2/\text{MoS}_2$  ( $T = \text{F, O, OH}$ ) [37].

Recently, a series of high-quality metallic TMDs (m-TMD)/semiconducting TMDs (s-TMD) vdW heterostructures with unusual electronic and photonic properties, such as  $\text{VSe}_2/\text{WSe}_2$ ,  $\text{NiTe}_2/\text{WSe}_2$ ,  $\text{CoTe}_2/\text{WSe}_2$ ,  $\text{VS}_2/\text{WSe}_2$ ,  $\text{VSe}_2/\text{MoS}_2$ , and  $\text{WSe}_2/\text{CrSe}_2$ , has been experimentally synthesized by chemical vapor deposition [23,24], which provides an option for solving the problems existing at the metal-semiconductor interface. Among these heterostructures, the  $\text{WSe}_2/\text{CrSe}_2$  heterostructure is an emerging vdW heterostructure with fascinating properties such as good environmental stability, high-quality vdW interfaces with clearly resolved moiré superlattices, and ferromagnetic (FM) behavior [24]. Moreover, the charge transfer from the  $\text{WSe}_2$  substrate has an important influence on the properties of  $\text{CrSe}_2$  in the heterostructure [24]. Additionally,  $\text{WSe}_2$  is a promising material for applications in  $p$ -type field-effect transistors owing to its perfect subthreshold swing and large  $I_{\text{ON}}/I_{\text{OFF}}$  values, while the relatively low carrier mobility and high contact resistance limit its applications [39]. Considering that  $\text{CrSe}_2$  displays a metallic character and intriguing magnetic behavior [40], the combination of  $\text{WSe}_2$  and  $\text{CrSe}_2$  to construct the  $\text{WSe}_2/\text{CrSe}_2$  heterostructure can be expected to exhibit more attractive properties and remedy the shortcomings existing in  $\text{WSe}_2$  by forming adjustable metal-semiconductor heterointerfaces. However, available studies on  $\text{WSe}_2/\text{CrSe}_2$  are limited to magnetically induced valley splitting, spin-filtering, and tunneling magnetoresistance in heterojunction [41,42]. Detailed knowledge about the electronic and magnetic properties of  $\text{WSe}_2/\text{CrSe}_2$  vdW heterostructure is still lacking. Furthermore, it remains unknown how strain can effectively modulate these properties and whether it can induce the transitions between different magnetic orders and/or between contact types.

In this paper, the geometric, electronic, and magnetic properties of the  $\text{WSe}_2/\text{CrSe}_2$  vdW heterostructure were systematically investigated by using density functional theory (DFT) calculations. Firstly, we investigated the geometric and electronic structures as well as magnetic ground states of the unstrained  $\text{WSe}_2/\text{CrSe}_2$  heterostructure. Subsequently, we explored its electronic and magnetic properties at different strains and examined the effects of interlayer and in-plane strains on these properties. Further, the strain-modulated interfacial contact properties of the heterostructure were characterized in terms of the Schottky barrier. Lastly, the effects of strain on tunneling capability of the heterostructure were discussed. This paper is structured as follows. A brief description of the computational methodology is given in the next section. The third section presents the computational results and discussion. The main conclusions are summarized in the fourth section.

## II. COMPUTATIONAL METHODS

All calculations in this paper were carried out by using first-principles calculations based on the spin-polarized DFT within the projector augmented-wave method [43], as implemented in VASP. The Perdew-Burke-Ernzerhof functional in the generalized gradient approximation was employed to

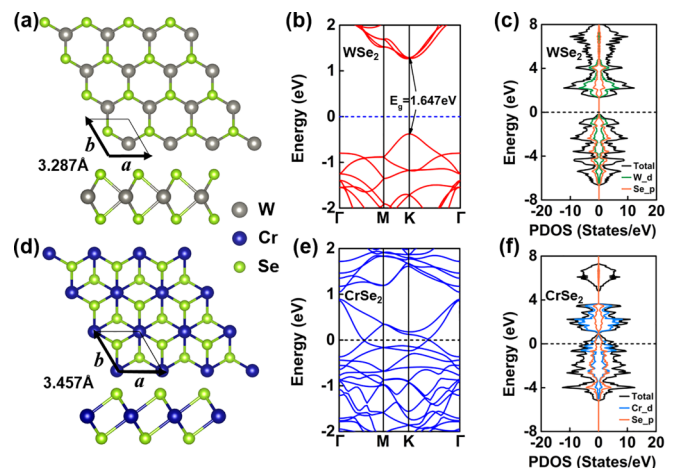


FIG. 1. Top and side views of (a)  $\text{WSe}_2$  and (d)  $\text{CrSe}_2$  monolayers. Black rhombuses in (a) and (d) refer to the unit cells of  $\text{WSe}_2$  and  $\text{CrSe}_2$ . Band structures of (b)  $\text{WSe}_2$  and (e)  $\text{CrSe}_2$  monolayers. Projected density of states (PDOS) of (c)  $\text{WSe}_2$  and (f)  $\text{CrSe}_2$  monolayers.

describe the electron exchange-correlation interactions [44]. A DFT-D2 method based on the Grimme scheme was used to describe the vdW correction between the  $\text{WSe}_2$  and  $\text{CrSe}_2$  monolayers. The kinetic energy cutoff was set to be 550 eV. Because of the application of periodic boundary conditions, a vacuum layer with a thickness of 20 Å was added along the Z direction to eliminate the interactions between neighboring layers. The Brillouin zone samplings for structural relaxations and electronic structure calculations were respectively set to be  $7 \times 7 \times 1$  and  $11 \times 11 \times 1$   $\Gamma$ -centered Monkhorst-Pack  $k$  mesh. All the initial structures were fully relaxed until the fluctuations for total energy and Hellmann-Feynman forces were  $< 10^{-6}$  eV and 0.01 eV/Å, respectively. In addition, a dipole correction along the Z direction was applied in all electrostatic potential calculations.

## III. RESULTS AND DISCUSSION

### A. Geometric and electronic structures of pristine states

Firstly, we investigated the structural and electronic properties of  $\text{WSe}_2$  and  $\text{CrSe}_2$  monolayers. As is well known, TMD layered materials have two common structures, i.e., trigonal prismatic  $2H$  and octahedral  $1T$  phases. The  $2H$  phase is a honeycomb structure with  $D_{3h}$  point group symmetry, and the  $1T$  phase is a central honeycomb structure with  $D_{3d}$  symmetry. According to experimental and theoretical verification,  $2H$ - $\text{WSe}_2$  and  $1T$ - $\text{CrSe}_2$  are considered the most stable, respectively [24,45]. Therefore, they are addressed in this paper. After full relaxation, the corresponding lattice constants are 3.287 and 3.457 Å [see Figs. 1(a) and 1(d) for specific configurations], in agreement with the available reports (3.32 and 3.46 Å) [41,46]. The bond lengths are 2.537 Å for W-Se and 2.501 Å for Cr-Se. For the  $\text{WSe}_2$  monolayer, the valence band maximum (VBM) and conduction band minimum (CBM) lie at the same  $\Gamma$  point [see Fig. 1(b)], indicating a nonmagnetic semiconductor with a direct band gap of 1.647 eV. To explore the electronic structure of the  $\text{CrSe}_2$  monolayer, we first

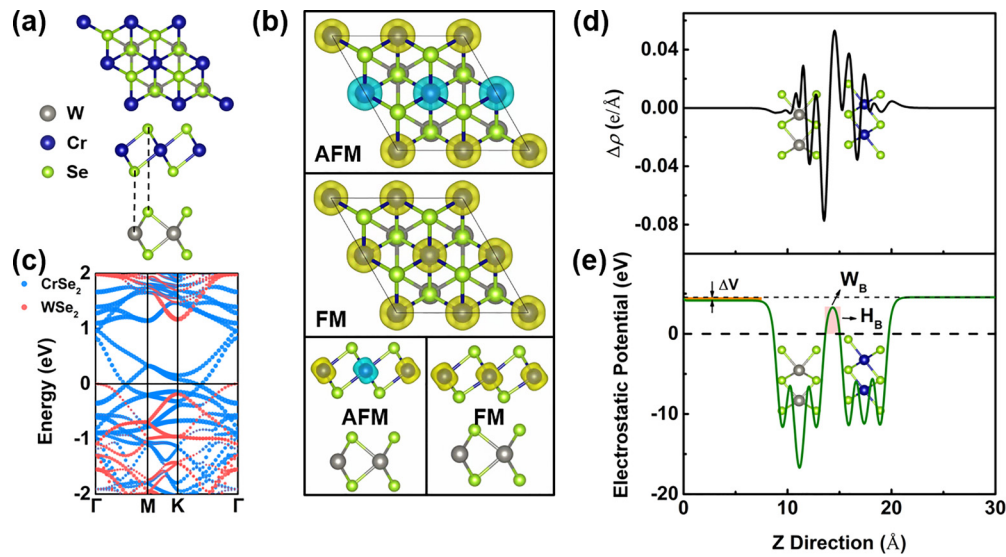


FIG. 2.  $\text{WSe}_2/\text{CrSe}_2$  heterostructure: (a) Relaxed structure (Configuration I), (b) spin densities in antiferromagnetic (AFM) and ferromagnetic (FM) states. The yellow and cyan isosurfaces refer to spin-up and spin-down densities, respectively, (c) projected band structure, (d) planar electronic density difference  $\Delta\rho$ , and (e) electrostatic potential along the  $Z$  direction.

investigated its magnetic ground state. A  $2 \times 2$  supercell of four Cr atoms was used, and both the FM and antiferromagnetic (AFM) states were considered (see Fig. S1 in the Supplemental Material (SM) [47] for details). The DFT calculations show that the energy of  $-7.149$  meV/unit cell for the AFM state is lower than that for the FM state, implying that the  $\text{CrSe}_2$  monolayer should display the AFM ground state. Moreover, the magnetic moments are mainly contributed by Cr atoms. These results are consistent with the previous study [40]. Further, the band structure and electronic state density of the  $\text{CrSe}_2$  monolayer in the AFM ground state are respectively illustrated in Figs. 1(e) and 1(f). Evidently, the bands and the electronic states of Cr  $-4d$  and Se  $-3p$  orbitals pass through the Fermi level, signifying the pronounced metallicity of  $\text{CrSe}_2$  monolayer.

The  $\text{WSe}_2/\text{CrSe}_2$  heterostructure consists of a  $2 \times 2$  primitive unit cell of the  $\text{WSe}_2$  monolayer and a  $2 \times 2$  primitive unit cell of the  $\text{CrSe}_2$  monolayer. According to the formula  $\delta = 2(a - b)/(a + b)$ , where  $a$  and  $b$  are the lattice constants of the two monolayers, the lattice mismatch between the monolayers is 5% or so. The small lattice mismatch is beneficial to a stable formation of the  $\text{WSe}_2/\text{CrSe}_2$  heterostructure. For screening the most stable  $\text{WSe}_2/\text{CrSe}_2$  heterostructure, six possible vertical stackings were considered, as labeled I–VI in Fig. S2 in the SM [47]. In these stacked heterostructures, we set the lattice constants of the  $\text{WSe}_2$  and  $\text{CrSe}_2$  layers to their average value ( $6.743 \text{ \AA}$ ). The total energies were minimized with respect to the in-plane lattice constant. After structural optimization, the  $\text{WSe}_2/\text{CrSe}_2$ -I stacking was found to be the most energetically stable, in agreement with the configuration in previous reports [41,42]. Its vertical distance of  $3.053 \text{ \AA}$  between interlayer surface atoms is also the smallest among all six configurations (see Tables S1 and S2 in the SM [47] for details about the total energy and structural information).

To evaluate the structural stability of the  $\text{WSe}_2/\text{CrSe}_2$ -I stacking in Fig. 2(a), we calculated its binding energy by the

following equation:

$$E_b = E_{\text{WSe}_2/\text{CrSe}_2} - E_{\text{WSe}_2} - E_{\text{CrSe}_2}, \quad (1)$$

where  $E_{\text{WSe}_2/\text{CrSe}_2}$  is the total energy of the heterostructure and  $E_{\text{WSe}_2}$  (or  $E_{\text{CrSe}_2}$ ) is the energy of pristine  $\text{WSe}_2$  (or  $\text{CrSe}_2$ ) monolayer. The binding energy of  $-1.241$  eV indicates that the  $\text{WSe}_2/\text{CrSe}_2$ -I heterostructure should be stable. Thus,  $\text{WSe}_2/\text{CrSe}_2$  is used to refer to the I-type stacking configuration in the following discussion. Like the  $\text{CrSe}_2$  monolayer, the  $\text{WSe}_2/\text{CrSe}_2$  heterostructure is also AFM at the ground state, and the energy difference between the AFM and FM states is  $-57$  meV/u.c., implying that the introduction of  $\text{WSe}_2$  does not change the magnetic state of  $\text{CrSe}_2$ . The spin densities of the  $\text{WSe}_2/\text{CrSe}_2$  heterostructure in the AFM and FM states are illustrated in Fig. 2(b). Evidently, the spin polarization in both magnetic states is solely attributed to Cr atoms. Figure 2(c) further illustrates the projected band structure of the  $\text{WSe}_2/\text{CrSe}_2$  heterostructure, where the contributions of  $\text{WSe}_2$  and  $\text{CrSe}_2$  are respectively marked in red and blue. The  $\text{WSe}_2/\text{CrSe}_2$  heterostructure exhibits metallic character, and the projected bands of the  $\text{CrSe}_2$  part are consistent with those of the  $\text{CrSe}_2$  monolayer. In contrast, the band gap of the  $\text{WSe}_2$  part is smaller than that of its monolayer, and the VBM shifts from the  $K$  point to the  $\Gamma$  point, suggesting a direct-to-indirect band gap transition induced by the formation of the heterostructure.

The interfacial characteristics and contact type (Schottky or ohmic) of metal-semiconductor interfaces are important factors to affect the carrier transport between metal and semiconductor and hence to determine the performance of heterostructures in practical applications. The specific type of contact and the Schottky barrier are usually determined based on the Fermi level and band edge of the semiconductor at the metal-semiconductor junction [34,37]. When the VBM or CBM of the semiconductor crosses the Fermi level, an ohmic contact is formed. Otherwise, a Schottky contact can be identified when the Fermi level lies between the VBM



and CBM of the semiconductor. Specifically, the CBM being close to the Fermi level indicates an  $n$ -type Schottky contact (nSC), while the VBM being close to the Fermi level signifies a  $p$ -type Schottky contact (pSC). Based on the Schottky-Mott model at the metal-semiconductor interface [48], the heights of  $n$ - and  $p$ -type Schottky barriers are respectively defined by

$$\Phi_N = E_{\text{CBM}} - E_F, \quad \Phi_P = E_F - E_{\text{VBM}}, \quad (2)$$

where  $E_F$  is the energy of the Fermi level, and  $E_{\text{CBM}}$  and  $E_{\text{VBM}}$  are the energies of the CBM and VBM, respectively.

As can be seen from Fig. 2(c), the VBM of WSe<sub>2</sub> partly contacts with the Fermi level; thus, the WSe<sub>2</sub>/CrSe<sub>2</sub> heterostructure exhibits a  $p$ -type ohmic contact (pOC). As shown in Table S3 and Fig. S3 in the SM [47], the use of DFT+ $U$  did not change the AFM ground state and the ohmic contact of the heterostructure. This contact type formed in the heterostructure is generally considered to have low contact resistance and is therefore beneficial for current input. Consequently, the WSe<sub>2</sub>/CrSe<sub>2</sub> vdW heterostructure is more suitable for application in  $p$ -type field-effect transistors than the WSe<sub>2</sub> monolayer with metals in which the Schottky contact is formed [49].

In the WSe<sub>2</sub>/CrSe<sub>2</sub> heterostructure, electron transfer occurs at the interface due to the difference in work function ( $W_F$ ) between the WSe<sub>2</sub> and CrSe<sub>2</sub> monolayers. Generally, the direction of electron transfer is from the layer with small  $W_F$  to the layer with large  $W_F$ . Hence, the electrons will transfer from WSe<sub>2</sub> ( $W_F = 5.088$  eV) to CrSe<sub>2</sub> ( $W_F = 5.584$  eV) in the WSe<sub>2</sub>/CrSe<sub>2</sub> heterostructure. To visualize the charge redistribution and charge transfer between the WSe<sub>2</sub> and CrSe<sub>2</sub> layers, we calculate the charge density difference as follows:

$$\Delta\rho = \rho_{\text{WSe}_2/\text{CrSe}_2} - \rho_{\text{WSe}_2} - \rho_{\text{CrSe}_2}, \quad (3)$$

where  $\rho_{\text{WSe}_2/\text{CrSe}_2}$ ,  $\rho_{\text{WSe}_2}$ , and  $\rho_{\text{CrSe}_2}$  are the charge densities of the WSe<sub>2</sub>/CrSe<sub>2</sub> heterostructure and pristine WSe<sub>2</sub> and CrSe<sub>2</sub> monolayers, respectively. As shown in Fig. 2(d), the charges accumulate near the CrSe<sub>2</sub> layer, whereas they deplete near the WSe<sub>2</sub> layer, implying that the charges are mainly transferred from the WSe<sub>2</sub> to the CrSe<sub>2</sub> layer. In addition, the Bader charge analysis suggests that the WSe<sub>2</sub> layer transfers 0.057 electron to the CrSe<sub>2</sub> layer. Due to the charge transfer, a built-in electric field can be created at the interface. Figure 2(e) illustrates the electrostatic potential of the WSe<sub>2</sub>/CrSe<sub>2</sub> heterostructure, with a potential difference  $\Delta V$  of 0.41 eV on two sides. Also, the interlayer dipole moment of the heterostructure is ascertained to be  $0.088 e \text{ \AA}$ .

### B. Strain-modulated magnetic properties

To further extend the applications of 2D vdW heterostructures, inducing (either interlayer or in-plane) strain is frequently considered an effective way to modulate their intrinsic properties and thus meet different application requirements. Therefore, we examined how the electronic and magnetic properties of the WSe<sub>2</sub>/CrSe<sub>2</sub> heterostructure are modulated by strain engineering. As shown in Fig. S4(a) in the SM [47], the interlayer strain was applied by changing the interlayer distance between the WSe<sub>2</sub> and CrSe<sub>2</sub> layers. The magnitude of the interlayer strain is defined as  $\varepsilon_D = \Delta D/D_0$ , where  $D_0$  and  $\Delta D$ , respectively, represent the interlayer distance of the unstrained WSe<sub>2</sub>/CrSe<sub>2</sub> heterostructure and its

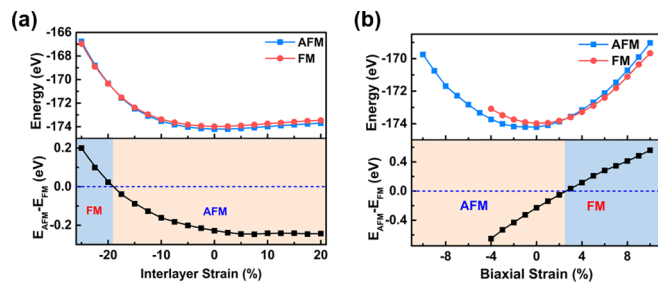


FIG. 3. (a) Total energy of WSe<sub>2</sub>/CrSe<sub>2</sub> heterostructure in antiferromagnetic (AFM) and ferromagnetic (FM) states at different interlayer strains and the energy difference between the two states. (b) Total energy of WSe<sub>2</sub>/CrSe<sub>2</sub> heterostructure in the AFM and FM states and the energy difference between the two states as a function of biaxial strain.

variation under interlayer strain. In the strained regime, the Z coordinates of W and Cr atoms were fixed, while Se atoms were fully relaxed. Note that the negative value of  $\varepsilon_D$  indicates the compressive strain. The total energies in the FM and AFM states and their difference ( $\Delta E = E_{\text{AFM}} - E_{\text{FM}}$ ) for different interlayer distances are presented in Fig. 3(a). Evidently, the energy difference between the AFM and FM states is negative in a large range of interlayer strains, implying that the WSe<sub>2</sub>/CrSe<sub>2</sub> heterostructure tends to be in the AFM ground state. However, with the interlayer compressive strain rising to  $-19\%$  (corresponding to small interlayer spacing), the total energy of the heterostructure in the FM state begins to be lower than that in the AFM state, signifying an AFM-to-FM transition in the heterostructure at this critical strain.

In addition, we explored the effect of in-plane biaxial strain, including compressive and tensile strains by decreasing and increasing the lattice parameter of the WSe<sub>2</sub>/CrSe<sub>2</sub> heterostructure. The in-plane strain can be expressed as  $\varepsilon_a = \Delta a/a_0$ , where the lattice constants of the unstrained and strained heterostructures are respectively denoted as  $a_0$  and  $a$  ( $a = a_0 - \Delta a$ ). The schematic illustration of the heterostructure under biaxial strain is displayed in Fig. S4(b) in the SM [47]. Similarly, we calculated the total energy of the WSe<sub>2</sub>/CrSe<sub>2</sub> heterostructure in the AFM and FM states under in-plane biaxial strain and the corresponding energy difference between the AFM and FM states to determine the magnetism of the ground state, as illustrated in Fig. 3(b). Clearly, the magnetism of the heterostructure is strongly dependent on the biaxial strain. It always remains an AFM ordered state under compressive strain, whereas when the tensile strain exceeds 2.5%, the positive energy difference occurs, meaning that the heterostructure transforms into an FM-favored ground state.

Next, the intrinsic mechanism of the magnetic order transition is discussed. It is known that the magnetic ground state of the CrSe<sub>2</sub> monolayer has been determined by the competition between direct-exchange and superexchange interactions of the two nearest-neighboring Cr atoms [40]. In the case of the WSe<sub>2</sub>/CrSe<sub>2</sub> heterostructure, the changes in Bader charge and interface dipole moment were calculated when it was subjected to two types of strains. As presented in Fig. S5 in the SM [47], the charge transfer and the interfacial dipole moment exhibit a similar trend, that is, they decrease with

increasing interlayer distance, while they increase with in-plane strain. The interlayer charge transfer of the  $\text{WSe}_2/\text{CrSe}_2$  heterostructure increases with the interlayer compressive strain and in-plane tensile strain, accompanied by the transition from the AFM to the FM state. However, it should be noted that the change in charge transfer is not the underlying cause of the magnetic transition because the same modulation pattern in the heterostructure is also found in the  $\text{CrSe}_2$  monolayer subjected to in-plane biaxial strain [40]. The magnetic moments of Cr atoms in the heterostructure and the  $\text{CrSe}_2$  monolayer under biaxial strain are respectively listed in Tables S4 and S5 in the SM [47]. It is found that the magnetic moment of each Cr atom in the former ( $2.357 \mu_B$ ) is approximately equal to that of the latter ( $2.360 \mu_B$ ), and both rise with increasing biaxial strain. The same trend and close magnetic moment further verify that, in the  $\text{WSe}_2/\text{CrSe}_2$  heterostructure, the magnetic properties of  $\text{CrSe}_2$  are not remarkably affected by the  $\text{WSe}_2$  layer. Consequently, the magnetic order transition in the heterostructure should still be attributed to the competition of exchange interactions.

It is known that the strength of the exchange interaction is closely associated with the distance between Cr atoms and the distance between Cr and neighboring Se atoms. To explore the mechanism of the transition between the AFM and FM states, the variation of atomic distances under two types of strains was analyzed. When changing the interlayer distance, the distance between neighboring Cr atoms ( $d_{\text{Cr-Cr}}$ ) is essentially constant, and thus, the strength of the direct AFM interaction also remains unchanged. However, the bond lengths between Cr and Se atoms on the upper and lower surfaces with interlayer coupling in the  $\text{CrSe}_2$  layer (see  $d_{\text{Cr-Se-up}}$  and  $d_{\text{Cr-Se-down}}$  in Fig. S4(a) in the SM [47]) vary remarkably with the interlayer distance. As shown in Fig. S6(a) in the SM [47],  $d_{\text{Cr-Se-down}}$  is contracted with the decreasing interlayer distance, causing the superexchange FM interaction to enhance. As the interlayer compression proceeds, the superexchange FM interaction gradually exceeds the direct AFM interaction, eventually leading to an AFM-to-FM transition. The results in Fig. 3(a) indicate that the magnetic ground state of the  $\text{WSe}_2/\text{CrSe}_2$  heterostructure has a low sensitivity to the interlayer coupling since a considerable interlayer compressive strain ( $-19\%$ ) is required to trigger the transition from the AFM to the FM state, which is consistent with the small change in the magnetic moment of Cr atoms (see Table S6 in the SM [47]). Next, the distance between Cr atoms ( $d_{\text{Cr-Cr}}$ ) and the distance between Cr and Se atoms ( $d_{\text{Cr-Se}}$ ) under different biaxial strains are illustrated in Fig. S6(b) in the SM [47]. It can be observed that the variation of  $d_{\text{Cr-Se}}$  with biaxial strain is small, indicating the basically unchanged superexchange FM interaction. By comparison,  $d_{\text{Cr-Cr}}$  increases linearly with biaxial strain, and the corresponding AFM direct-exchange interaction gradually decreases, leading to the dominance of superexchange FM interaction. As a result, the transition from the AFM to the FM state occurs in the  $\text{CrSe}_2$  layer of the heterostructure.

### C. Strain-modulated electronic properties

From the device point of view, the contact type of metal-semiconductor interface is crucial for the applications of the

$\text{WSe}_2/\text{CrSe}_2$  vdW heterostructure. As disclosed in Sec. III A, it exhibits pOC in a pristine state. Here, we further explore whether the contact type and the Schottky barrier of such a heterostructure can be tuned by interlayer and in-plane biaxial strain. As demonstrated in the previous magnetic analysis, under interlayer strains, the  $\text{WSe}_2/\text{CrSe}_2$  vdW heterostructure mostly remains in the AFM ground state. However, as the interlayer compressive strains become  $> -19\%$ , the large reduction in the layer spacing of the heterostructure in the FM state leads to an increase in the repulsive forces between the Se atoms at the interface, with a consequent severe distortion of the structure of  $\text{CrSe}_2$ . Therefore, the interlayer strain is only applied up to  $-25\%$ . Here, the effects of the interlayer strain in the AFM state on the type of interfacial contact and Schottky barrier are first chosen to be discussed. Figure 4(a) shows the projected band structures of the  $\text{WSe}_2/\text{CrSe}_2$  heterostructure under different interlayer strains, and the detailed information on CBM and VBM variations is illustrated in Fig. 4(b). It is observed that the band structure of the  $\text{CrSe}_2$  part essentially remains unchanged. In contrast, the  $\text{WSe}_2$  part is remarkably affected by the interlayer coupling, leading to significant changes in the contact type and the barrier height. With the interlayer tensile strain increasing from 0 to 20%, the overall energy levels of the conduction and valence bands of  $\text{WSe}_2$  located at the  $K$  point shift upward, whereas the energy level of the valence band located at the  $\Gamma$  point shifts downward. The VBM shifts from the  $\Gamma$  to the  $K$  point at the interlayer strain of 10%, indicating that the band structure of  $\text{WSe}_2$  in the heterostructure changes from an indirect to a direct band gap. By contrast, with the interlayer compressive strain going from 0 to  $-17.5\%$ , the energy levels of the conduction and valence bands of  $\text{WSe}_2$  located at the  $K$  point move downward as a whole, while the energy level of the VBM located at the  $\Gamma$  point moves upward and crosses the Fermi level. Note that the contribution of  $\text{WSe}_2$  to the valence band which crosses the Fermi level gradually diminishes with the increasing interlayer compressive strain and almost disappears at the strain of  $-13\%$ . When the interlayer distance further decreases, this band is solely contributed by  $\text{CrSe}_2$ . These results demonstrate that large compression can induce the transition from ohmic to Schottky contact in the  $\text{WSe}_2/\text{CrSe}_2$  heterointerface.

To gain a deep understanding of the mechanisms of interlayer coupling, we calculated the Schottky barrier at different strains according to Eq. (2), and the corresponding results are presented in Fig. 4(c). The  $n$ -type Schottky barrier decreases with the interlayer compressive strain. However, the  $p$ -type Schottky barrier first decreases and then abruptly increases. It becomes positive at the compressive strain of  $-13\%$ , where the contribution of  $\text{WSe}_2$  to the valence band crossing the Fermi level disappears, indicating the switching from pOC to pSC. Moreover, the  $n$ -type Schottky barrier becomes less than the  $p$ -type Schottky barrier as the compressive strain continues to increase to  $-15.5\%$ , implying that the heterostructure switches to nSC. That is, applying interlayer compressive strain (increasing interlayer coupling) at the interface of the  $\text{WSe}_2/\text{CrSe}_2$  heterostructure can induce a continuous transition from pOC to pSC and nSC, suggesting that inducing interlayer strain is an effective way to efficiently modulate the contact type and Schottky barrier at the heterointerface.

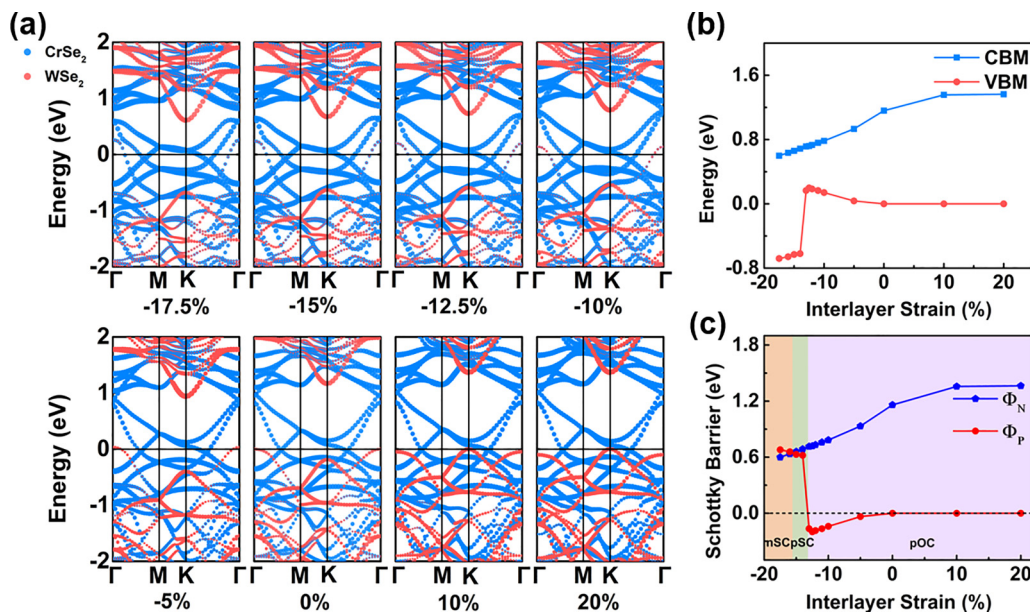


FIG. 4. (a) Projected band structures of  $\text{WSe}_2/\text{CrSe}_2$  heterostructure under different interlayer strains. The red part represents the contribution of  $\text{WSe}_2$  supercell, and the blue part represents the contribution of  $\text{CrSe}_2$  supercell. (b) Band edge position and (c) Schottky barrier of  $\text{WSe}_2/\text{CrSe}_2$  heterostructure as a function of interlayer strain.

In addition, the band structure of the FM state evolved with the interlayer compressive strain ranging from  $-25$  to  $20\%$  is illustrated in Fig. S7 in the SM [47]. The spin-up band structures remain nSC, and the spin-down ones exhibit pOC.

Next, the effects of in-plane biaxial strain on the interfacial properties of the  $\text{WSe}_2/\text{CrSe}_2$  heterostructure are discussed. From our analyses of the magnetism at ground states, it can be found that the  $\text{WSe}_2/\text{CrSe}_2$  heterostructure exhibits the AFM state at biaxial strain ranging from  $-10$  to  $2.5\%$  [see Fig. 3(b)]. Hence, the AFM states of the heterostructure were addressed to explore the influence of the in-plane biaxial strain on the contact type of interface and the Schottky barrier. As shown in Fig. 5, the biaxial compressive strain can tune the interfacial contact of the  $\text{WSe}_2/\text{CrSe}_2$  heterostructure from pOC to pSC. Both  $n$ - and  $p$ -type Schottky barriers significantly depend on the strain. A clear difference between them, however, can be identified. That is, the latter gradually increases with the increasing biaxial compressive strain, while the former tends to increase and then decrease, as indicated by Fig. 5(a). From the band structures illustrated in Figs. 5(b) and 5(c), one can find that when the biaxial compressive strain goes from  $0$  to  $-2\%$ , the CBM of the  $\text{WSe}_2$  part in the heterostructure moves upward, while the VBM moves downward. The VBM shifts from the  $\Gamma$  to the  $K$  point at the strain of  $-2\%$ , signifying the occurrence of the indirect-to-direct band gap transition. Subsequently, the CBM shifts downward with biaxial compressive strains further ranging from  $-2$  to  $-10\%$ , suggesting that the tendency of the CBM to increase and then decrease may be related to the change in the type of band alignment from indirect to direct band gap. The above results indicate that the biaxial compressive strain can effectively modulate the interfacial contact type and the Schottky barrier. Additionally, we also calculated the band structure of the  $\text{WSe}_2/\text{CrSe}_2$  heterostructure in the FM state under biaxial tensile strain (see Fig. S8 in the SM [47]). In

this case, no significant change in the overall properties of the heterostructure is observed, despite the shifting band structure of the  $\text{WSe}_2$  part.

#### D. Characterization of strain-modulated tunneling capability

For metal-semiconductor heterostructures, in addition to the Schottky barrier, the tunneling barrier is another important parameter to measure the interface performance, which can reflect the efficiency of carrier injection and transport at the metal-semiconductor interface [38]. Generally, high tunneling potential barriers facilitate the carrier injection, while low tunneling potential barriers may promote the carrier transport across the interface. It is usually reflected through the tunneling probability ( $T_B$ ), which is defined by barrier height ( $H_B$ ) and barrier width ( $W_B$ ). When the square barrier model is adopted,  $T_B$  can be evaluated by the formula [50,51]:

$$T_B = \exp\left(-2\frac{\sqrt{2mH_B}}{\hbar}W_B\right), \quad (4)$$

where  $m$  and  $\hbar$  are the free electron mass and Planck's constant, respectively. Meanwhile, we replaced the actual barrier at the  $\text{WSe}_2/\text{CrSe}_2$  interface in Fig. 2(d) with a squared barrier and measured its width ( $W_B$ ) and height ( $H_B$ ). The calculated tunneling probability of the unstrained  $\text{WSe}_2/\text{CrSe}_2$  heterostructure is  $7.88\%$ .

The low tunneling probability indicates a high tunneling barrier at the heterostructure interface, which is not favorable for carrier transportation. Available studies have demonstrated that the tunneling barrier and tunneling probability of  $\text{Ti}_3\text{X}_2/\text{MoS}_2$  ( $X = \text{B}, \text{C}, \text{N}$ ) heterostructures can be effectively modulated by varying the interlayer distance, and in-plane strain can also tune the tunneling probability of  $\text{Ti}_3\text{C}_2\text{T}_2/\text{MoS}_2$  ( $T = \text{F}, \text{O}, \text{OH}$ ) [37,38]. Inspired by these studies, we



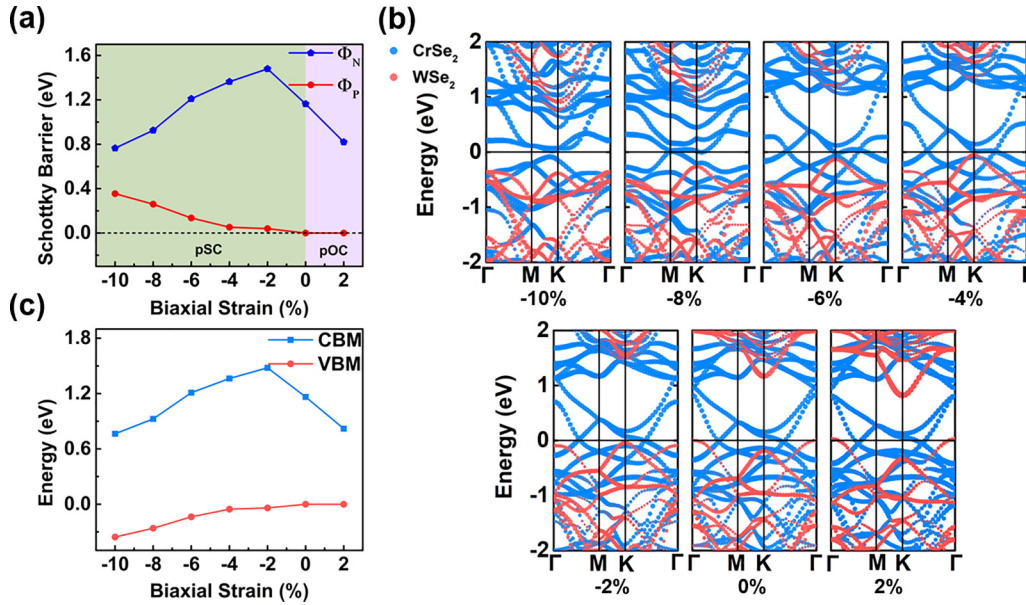


FIG. 5. (a) Schottky barrier of the heterostructure subjected to biaxial strain. (b) Projected band structures of WSe<sub>2</sub>/CrSe<sub>2</sub> heterostructure under different biaxial strains. The red and blue parts, respectively, represent the contributions from WSe<sub>2</sub> and CrSe<sub>2</sub> supercells. (c) Band edge position of the heterostructure subjected to biaxial strain.

further investigated the tunneling capability of the WSe<sub>2</sub>/CrSe<sub>2</sub> heterostructure under interlayer and in-plane biaxial strain to explore whether the two approaches can modulate its tunneling barrier. Figures 6(a) and 6(b) illustrate the electrostatic potentials of the WSe<sub>2</sub>/CrSe<sub>2</sub> heterostructure under two types of strains, from which the corresponding square barrier height and barrier width can be obtained

to detect the variation of the tunneling probability. It is observed from Fig. 6(c) that the interlayer strain has a large effect on the barrier height and width. With the increasing interlayer distance, both gradually rise while the tunneling probability drops accordingly. On the contrary, decreasing the interlayer distance makes the interfacial interactions increase. As a result, the barrier height and width drop significantly, corresponding to a large rise in the tunneling probability. At the interlayer strain of -20%, the tunneling probability even reaches 100%, indicating that the reduction of the interlayer distance is beneficial to increasing the tunneling probability of the interface, decreasing the interface tunneling barrier, and promoting the carrier transport capability at the interface. In contrast, the in-plane biaxial strain has a small effect on both the barrier height and width of the WSe<sub>2</sub>/CrSe<sub>2</sub> heterostructure, as indicated by Fig. 6(d). Simultaneously, a small tunneling probability can be observed from this figure, suggesting that the charge transfer from metal to semiconductor is still suppressed. Therefore, these results demonstrate that the tunneling barrier of the WSe<sub>2</sub>/CrSe<sub>2</sub> heterostructure is more sensitive to the interlayer strain and strongly depends on the interfacial interactions. Our results are like the modulation of the tunneling barrier in Ti<sub>2</sub>X<sub>2</sub>/MoS<sub>2</sub> heterostructures where a significant reduction of the tunneling barrier can be achieved by decreasing the interlayer distance [38], suggesting that the interlayer strain might serve as a feasible method to modulate the tunneling barrier in metal-semiconductor heterostructures. Therefore, for the WSe<sub>2</sub>/CrSe<sub>2</sub> heterostructure, the improvement of interfacial properties can be realized by adjusting the interlayer distance. For example, the interlayer distance can be appropriately decreased so that the heterostructure may both maintain the ohmic contact in favor of carrier injection and lower the tunneling barrier at the interface. In this way, the WSe<sub>2</sub>/CrSe<sub>2</sub> heterostructure can have a high carrier injection efficiency

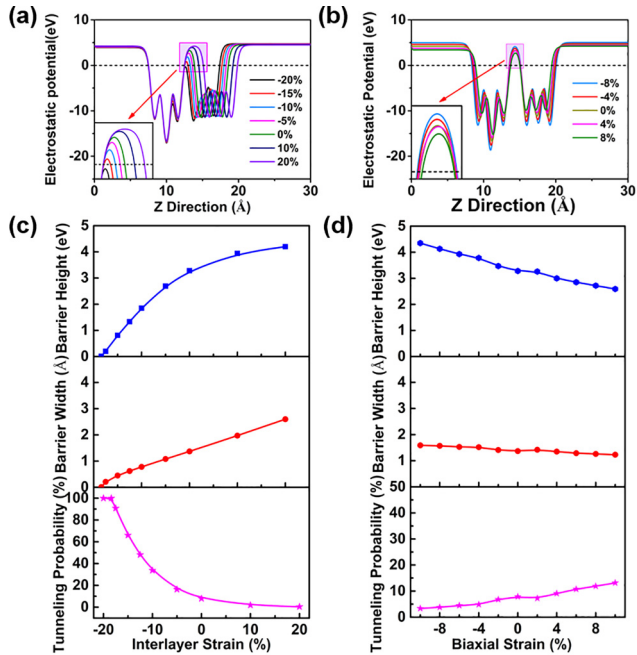


FIG. 6. The electrostatic potential of WSe<sub>2</sub>/CrSe<sub>2</sub> heterostructure along the Z direction at (a) interlayer and (b) biaxial strains. Barrier height, barrier width, and tunneling probability of the heterostructure at (c) interlayer and (d) biaxial strains.

along with desired interfacial carrier transport, which is favorable for current input and output. This makes it a potential candidate for future high-performance, low-power field-effect transistors. All in all, the  $\text{WSe}_2/\text{CrSe}_2$  heterostructure should be a promising 2D nanomaterial with tunable electronic and magnetic properties. From the perspective of device application, strain engineering is an effective way not only to effectively control the contact type and Schottky barrier at the interface but also to alter the tunneling characteristics at the interface, thus shedding light on strain regulation to enhance the performance of nanoelectronic devices.

#### IV. CONCLUSIONS

In summary, we investigated the geometric, electronic, and magnetic properties of the  $\text{WSe}_2/\text{CrSe}_2$  heterostructure by DFT calculations. The results show that  $\text{WSe}_2$  and  $\text{CrSe}_2$  can form a stable vdW heterostructure with an AFM ground state and metal-semiconductor interface. Like the pristine  $\text{CrSe}_2$  monolayer, the heterostructure can transform from the AFM into the FM state at in-plane biaxial strain exceeding 2.5%. By comparison, the magnetic order is insensitive to interlayer coupling, and a relatively high interlayer compressive strain (−19%) is required to induce the AFM-to-FM transition. The transition of the magnetic ground state is independent of the change in interfacial charge transfer. Furthermore, the pOC is found to form at the interface of the  $\text{WSe}_2/\text{CrSe}_2$  heterostructure, and both the interlayer and in-plane strain can effectively

modulate the interface contact type and the Schottky barrier height. Specifically, the contact type of the  $\text{WSe}_2/\text{CrSe}_2$  heterostructure can transform from pOC to pSC at interlayer strain of −13% and to nSC at −15.5%. Meanwhile, the transition of the  $\text{WSe}_2/\text{CrSe}_2$  heterostructure from pOC to pSC is also observed under in-plane biaxial compression. Additionally, a tunneling barrier exists at the heterostructure interface due to weak vdW interactions. With the decreasing interlayer distance, the enhancing interlayer interaction can lower the height and width of the tunneling barrier and consequently increase the tunneling probability, which in turn promotes the carrier transport capability at the interface. Therefore, the injection and transport efficiency of interface carriers can be controlled by adjusting the interlayer distance to optimize the current input and output. In this paper, we not only advance the fundamental understanding on strain-modulated electronic and magnetic properties of the  $\text{WSe}_2/\text{CrSe}_2$  vdW heterostructure but also provide important reference for designing and developing Schottky devices or low-power field-effect transistors based on vdW heterostructures.

#### ACKNOWLEDGMENTS

This paper was financially supported by the Natural Science Foundation of Fujian Province of China (Grant No. 2022J02001) and the Fundamental Research Funds for the Central Universities of China (Grant No. 20720220028). High Performance Computing Center of Xiamen University was acknowledged for the supercomputer resources.

- 
- [1] K. S. G. Novoselov, A. K. Geim, S. V. Morozov, D. Jiang, Y. Zhang, S. V. Dubonos, I. V. Grigorieva, and A. A. Firsov, Electric field effect in atomically thin carbon films, *Science* **306**, 666 (2004).
  - [2] D. Pacilé, J. C. Meyer, Ç. Ö. Girit, and A. Zettl, The two-dimensional phase of boron nitride: Few-atomic-layer sheets and suspended membranes, *Appl. Phys. Lett.* **92**, 133107 (2008).
  - [3] C. Xia, W. Xiong, J. Du, T. Wang, Y. Peng, and J. Li, Universality of electronic characteristics and photocatalyst applications in the two-dimensional Janus transition metal dichalcogenides, *Phys. Rev. B* **98**, 165424 (2018).
  - [4] K. S. Novoselov, A. Mishchenko, A. Carvalho, and A. H. Castro Neto, 2D materials and van der Waals heterostructures, *Science* **353**, aac9439 (2016).
  - [5] F. Xia, H. Wang, D. Xiao, M. Dubey, and A. Ramasubramaniam, Two-dimensional material nanophotonics, *Nat. Photonics* **8**, 899 (2014).
  - [6] C. Tan, X. Cao, X. J. Wu, Q. He, J. Yang, X. Zhang, J. Chen, W. Zhao, S. Han, G. H. Nam *et al.*, Recent advances in ultrathin two-dimensional nanomaterials, *Chem. Rev.* **117**, 6225 (2017).
  - [7] Y. Xiao, M. Zhou, J. Liu, J. Xu, and L. Fu, Phase engineering of two-dimensional transition metal dichalcogenides, *Sci. China Mater.* **62**, 759 (2019).
  - [8] Y. Wang, S. Zhao, Y. Wang, D. A. Laleyan, Y. Wu, B. Ouyang, P. Ou, J. Song, and Z. Mi, Wafer-scale synthesis of monolayer  $\text{WSe}_2$ : A multi-functional photocatalyst for efficient overall pure water splitting, *Nano Energy* **51**, 54 (2018).
  - [9] I. Eren, F. Iyikanat, and H. Sahin, Defect tolerant and dimension dependent ferromagnetism in  $\text{MnSe}_2$ , *Phys. Chem. Chem. Phys.* **21**, 16718 (2019).
  - [10] D. C. Freitas, M. Núñez, P. Strobel, A. Sulpice, R. Weht, A. A. Aligia, and M. Núñez-Regueiro, Antiferromagnetism and ferromagnetism in layered 1T-CrSe<sub>2</sub> with V and Ti replacements, *Phys. Rev. B* **87**, 014420 (2013).
  - [11] C. Wang, X. Zhou, Y. Pan, J. Qiao, X. Kong, C.-C. Kaun, and W. Ji, Layer and doping tunable ferromagnetic order in two-dimensional CrS<sub>2</sub> layers, *Phys. Rev. B* **97**, 245409 (2018).
  - [12] A. Karbalae Aghaee, S. Belbasi, and H. Hadipour, *Ab initio* calculation of the effective Coulomb interactions in  $\text{MX}_2$  ( $M = \text{Ti, V, Cr, Mn, Fe, Co, Ni}$ ;  $X = \text{S, Se, Te}$ ): Intrinsic magnetic ordering and Mott phase, *Phys. Rev. B* **105**, 115115 (2022).
  - [13] C. Wang, X. Zhou, L. Zhou, Y. Pan, Z.-Y. Lu, X. Wan, X. Wang, and W. Ji, Bethe-Slater-curve-like behavior and interlayer spin-exchange coupling mechanisms in two-dimensional magnetic bilayers, *Phys. Rev. B* **102**, 020402(R) (2020).
  - [14] M. Alsubaie, C. Tang, D. Wijethunge, D. Qi, and A. Du, First-principles study of the enhanced magnetic anisotropy and transition temperature in a  $\text{CrSe}_2$  monolayer via hydrogenation, *ACS Appl. Electron. Mater.* **4**, 3240 (2022).
  - [15] K. F. Mak, C. Lee, J. Hone, J. Shan, and T. F. Heinz, Atomically thin  $\text{MoS}_2$ : A new direct-gap semiconductor, *Phys. Rev. Lett.* **105**, 136805 (2010).
  - [16] W. Wu, D. De, S.-C. Chang, Y. Wang, H. Peng, J. Bao, and S.-S. Pei, High mobility and high on/off ratio field-effect transistors



- based on chemical vapor deposited single-crystal MoS<sub>2</sub> grains, *Appl. Phys. Lett.* **102**, 142106 (2013).
- [17] A. K. Geim and I. V. Grigorieva, van der Waals heterostructures, *Nature (London)* **499**, 419 (2013).
- [18] D. K. Bediako, M. Rezaee, H. Yoo, D. T. Larson, S. Y. F. Zhao, T. Taniguchi, K. Watanabe, T. L. Brower-Thomas, E. Kaxiras *et al.*, Heterointerface effects in the electrointercalation of van der Waals heterostructures, *Nature (London)* **558**, 425 (2018).
- [19] B. Huang, G. Clark, E. Navarro-Moratalla, D. R. Klein, R. Cheng, K. L. Seyler, D. Zhong, E. Schmidgall, M. A. McGuire, D. H. Cobden *et al.*, Layer-dependent ferromagnetism in a van der Waals crystal down to the monolayer limit, *Nature (London)* **546**, 270 (2017).
- [20] T. Georgiou, R. Jalil, B. D. Belle, L. Britnell, R. V. Gorbachev, S. V. Morozov, Y. J. Kim, A. Gholinia, S. J. Haigh, O. Makarovskiy *et al.*, Vertical field-effect transistor based on graphene-WS<sub>2</sub> heterostructures for flexible and transparent electronics, *Nat. Nanotechnol.* **8**, 100 (2013).
- [21] D. Pierucci, H. Henck, J. Avila, A. Balan, C. H. Naylor, G. Patriarche, Y. J. Dappe, M. G. Silly, F. Sirotti, A. T. Johnson *et al.*, Band alignment and minigaps in monolayer MoS<sub>2</sub>-graphene van der Waals heterostructures, *Nano Lett.* **16**, 4054 (2016).
- [22] S. Liu, Z. Li, Y. Ge, H. Wang, R. Yue, X. Jiang, J. Li, Q. Wen, and H. Zhang, Graphene/phosphorene nano-heterojunction: Facile synthesis, nonlinear optics, and ultrafast photonics applications with enhanced performance, *Photonics Res.* **5**, 662 (2017).
- [23] J. Li, X. Yang, Y. Liu, B. Huang, R. Wu, Z. Zhang, B. Zhao, H. Ma, W. Dang, Z. Wei *et al.*, General synthesis of two-dimensional van der Waals heterostructure arrays, *Nature (London)* **579**, 368 (2020).
- [24] B. Li, Z. Wan, C. Wang, P. Chen, B. Huang, X. Cheng, Q. Qian, J. Li, Z. Zhang, G. Sun *et al.*, van der Waals epitaxial growth of air-stable CrSe<sub>2</sub> nanosheets with thickness-tunable magnetic order, *Nat. Mater.* **20**, 818 (2021).
- [25] Z. Zhang, Z. Huang, J. Li, D. Wang, Y. Lin, X. Yang, H. Liu, S. Liu, Y. Wang, B. Li *et al.*, Endoepitaxial growth of monolayer mosaic heterostructures, *Nat. Nanotechnol.* **17**, 493 (2022).
- [26] Y. Liu, J. Guo, E. Zhu, L. Liao, S.-J. Lee, M. Ding, I. Shakir, V. Gambin, Y. Huang, and X. Duan, Approaching the Schottky-Mott limit in van der Waals metal-semiconductor junctions, *Nature (London)* **557**, 696 (2018).
- [27] Z. Zhang, Y. Gong, X. Zou, P. Liu, P. Yang, J. Shi, L. Zhao, Q. Zhang, L. Gu, and Y. Zhang, Epitaxial growth of two-dimensional metal-semiconductor transition-metal dichalcogenide vertical stacks (VSe<sub>2</sub>/MX<sub>2</sub>) and their band alignments, *ACS Nano* **13**, 885 (2018).
- [28] A. Allain, J. Kang, K. Banerjee, and A. Kis, Electrical contacts to two-dimensional semiconductors, *Nat. Mater.* **14**, 1195 (2015).
- [29] K. D. Pham, N. N. Hieu, H. V. Phuc, B. D. Hoi, V. V. Ilysov, B. Amin, and C. V. Nguyen, First principles study of the electronic properties and Schottky barrier in vertically stacked graphene on the Janus MoSeS under electric field, *Comput. Mater. Sci.* **153**, 438 (2018).
- [30] Y. Kim, A. R. Kim, J. H. Yang, K. E. Chang, J.-D. Kwon, S. Y. Choi, J. Park, K. E. Lee, D.-H. Kim, S. M. Choi *et al.*, Alloyed 2D metal-semiconductor heterojunctions: Origin of interface states reduction and Schottky barrier lowering, *Nano Lett.* **16**, 5928 (2016).
- [31] T. Shen, A. V. Penumatcha, and J. Appenzeller, Strain engineering for transition metal dichalcogenides based field effect transistors, *ACS Nano* **10**, 4712 (2016).
- [32] I. Lee, W. T. Kang, Y. S. Shin, Y. R. Kim, U. Y. Won, K. Kim, D. L. Duong, K. Lee, J. Heo, Y. H. Lee *et al.*, Ultrahigh gauge factor in graphene/MoS<sub>2</sub> heterojunction field effect transistor with variable Schottky barrier, *ACS Nano* **13**, 8392 (2019).
- [33] A. P. John, A. Thenapparambil, and M. Thalakulam, Strain-engineering the Schottky barrier and electrical transport on MoS<sub>2</sub>, *Nanotechnology* **31**, 275703 (2020).
- [34] H. T. T. Nguyen, M. M. Obeid, A. Bafekry, M. Idrees, T. V. Vu, H. V. Phuc, N. N. Hieu, L. T. Hoa, B. Amin, and C. V. Nguyen, Interfacial characteristics, Schottky contact, and optical performance of a graphene/Ga<sub>2</sub>Sse van der Waals heterostructure: Strain engineering and electric field tunability, *Phys. Rev. B* **102**, 075414 (2020).
- [35] T. V. Vu, N. V. Hieu, H. V. Phuc, N. N. Hieu, H. D. Bui, M. Idrees, B. Amin, and C. V. Nguyen, Graphene/WSeTe van der Waals heterostructure: Controllable electronic properties and Schottky barrier via interlayer coupling and electric field, *Appl. Surf. Sci.* **507**, 145036 (2020).
- [36] R. Zhang, G. Hao, X. Ye, S. Gao, and H. Li, Tunable electronic properties and Schottky barrier in a graphene/WSe<sub>2</sub> heterostructure under out-of-plane strain and an electric field, *Phys. Chem. Chem. Phys.* **22**, 23699 (2020).
- [37] Y. Liu, Q. Zhang, W. Zhang, R. Zhang, B. Wang, C. Ji, Z. Pei, and S. Sang, Tuning Schottky barrier and contact type of metal-semiconductor in Ti<sub>3</sub>C<sub>2</sub>T<sub>2</sub>/MoS<sub>2</sub> (T = F, O, OH) by strain: A first-principles study, *J. Phys. Chem. C* **125**, 16200 (2021).
- [38] Y. Liu, W. Zhang, B. Lv, Y. Ge, R. Zhang, B. Wang, Z. Chen, Q. Zhang, and S. Sang, Interface transition from ohmic to Schottky contact in Ti<sub>3</sub>X<sub>2</sub>/MoS<sub>2</sub> (X = B, C, N): Insights from first-principles, *Surf. Interfaces* **30**, 101823 (2022).
- [39] J. H. Park, A. Rai, J. Hwang, C. Zhang, I. Kwak, S. F. Wolf, S. Vishwanath, X. Liu, M. Dobrowolska, J. Furdyna *et al.*, Band structure engineering of layered WSe<sub>2</sub> via one-step chemical functionalization, *ACS Nano* **13**, 7545 (2019).
- [40] H. Y. Lv, W. J. Lu, D. F. Shao, Y. Liu, and Y. P. Sun, Strain-controlled switch between ferromagnetism and antiferromagnetism in 1T-CrX<sub>2</sub> (X = Se, Te) monolayers, *Phys. Rev. B* **92**, 214419 (2015).
- [41] C. Jiang, Z. Yang, W. Xiong, and F. Wang, Effect of strain engineering on magnetism-induced valley splitting in WSe<sub>2</sub> based on the WSe<sub>2</sub>/CrSe<sub>2</sub> heterojunction, *Appl. Phys. Lett.* **119**, 162101 (2021).
- [42] J. Feng, K. Li, M. Zheng, W. Zhang, Y. Liu, D. Wang, Z. Zhang, C. Zuo, R. Xiong, and Z. Lu, Excellent spin-filtering and giant tunneling magnetoresistance in a dual-electrode van der Waals magnetic tunnel junction based on ferromagnetic CrSe<sub>2</sub>, *Appl. Surf. Sci.* **611**, 155588 (2023).
- [43] G. Kresse and J. Hafner, *Ab initio* molecular dynamics for liquid metals, *Phys. Rev. B* **47**, 558 (1993).
- [44] G. Kresse, Efficient iterative schemes for *ab initio* total-energy calculations using a plane-wave basis set, *Phys. Rev. B* **54**, 11169 (1996).

- [45] J. He, K. Hummer, and C. Franchini, Stacking effects on the electronic and optical properties of bilayer transition metal dichalcogenides MoS<sub>2</sub>, MoSe<sub>2</sub>, WS<sub>2</sub>, and WSe<sub>2</sub>, *Phys. Rev. B* **89**, 075409 (2014).
- [46] J. Ye, J. Liu, and Y. An, Electric field and strain effects on the electronic and optical properties of g-C<sub>3</sub>N<sub>4</sub>/WSe<sub>2</sub> van der Waals heterostructure, *Appl. Surf. Sci.* **501**, 144262 (2020).
- [47] See Supplemental Material at <http://link.aps.org/supplemental/10.1103/PhysRevMaterials.8.014003> for additional figures and tables.
- [48] W. Chen, E. J. G. Santos, W. Zhu, E. Kaxiras, and Z. Zhang, Tuning the electronic and chemical properties of monolayer MoS<sub>2</sub> adsorbed on transition metal substrates, *Nano Lett.* **13**, 509 (2013).
- [49] L. P. Feng, J. Su, and Z. T. Liu, Computational study of hafnium metal contacts to monolayer WSe<sub>2</sub>, *J. Alloys Compd.* **639**, 210 (2015).
- [50] X. Ji, J. Zhang, Y. Wang, H. Qian, and Z. Yu, A theoretical model for metal-graphene contact resistance using a DFT-NEGF method, *Phys. Chem. Chem. Phys.* **15**, 17883 (2013).
- [51] J. Liu, Y. Guo, F. Q. Wang, and Q. Wang, TiS<sub>3</sub> sheet based van der Waals heterostructures with a tunable Schottky barrier, *Nanoscale* **10**, 807 (2018).